UCLA
UCLA Previously Published Works

Title

Spatial multiomics of arterial regions from cardiac allograft vasculopathy rejected grafts reveal novel insights into the pathogenesis of chronic antibody-mediated rejection.

Permalink

https://escholarship.org/uc/item/3sp317fp

Journal

American Journal of Transplantation, 24(7)

Authors

Nevarez-Mejia, Jessica
Pickering, Harry
Sosa, Rebecca
et al.

Publication Date

2024-07-01

DOI

10.1016/j.ajt.2024.01.004

Copyright Information

This work is made available under the terms of a Creative Commons Attribution-NonCommercial-NoDerivatives License, available at https://creativecommons.org/licenses/by-nc-nd/4.0/

Peer reviewed

eScholarship.org Powered by the California Digital Library
University of California

Author Manuscript

Author Manuscript

Author Manuscript

Author Manuscript

HHS Public Access

Author manuscript

Am J Transplant. Author manuscript; available in PMC 2024 July 18.

Published in final edited form as:

Am J Transplant. 2024 July ; 24(7): 1146–1160. doi:10.1016/j.ajt.2024.01.004.

Spatial multiomics of arterial regions from cardiac allograft vasculopathy rejected grafts reveal novel insights into the pathogenesis of chronic antibody-mediated rejection

Jessica Nevarez-Mejia[1], **Harry Pickering**[1], **Rebecca A. Sosa**[1], **Nicole M. Valenzuela**[1], **Gregory A. Fishbein**[1], **William M. Baldwin III**[2], **Robert L. Fairchild**[2], **Elaine F. Reed**[1,*]

[1]Department of Pathology and Laboratory Medicine, University of California, Los Angeles, California, USA

[2]Department of Inflammation & Immunity, Lerner Research Institute, Cleveland Clinic, Cleveland, Ohio, USA

Abstract

Cardiac allograft vasculopathy (CAV) causes late graft failure and mortality after heart transplantation. Donor-specific antibodies (DSAs) lead to chronic endothelial cell injury, inflammation, and arterial intimal thickening. In this study, GeoMx digital spatial profiling was used to analyze arterial areas of interest (AOIs) from CAV+DSA+ rejected cardiac allografts (N = 3; 22 AOIs total). AOIs were categorized based on CAV neointimal thickening and underwent whole transcriptome and protein profiling. By comparing our transcriptomic data with that of healthy control vessels of rapid autopsy myocardial tissue, we pinpointed specific pathways and transcripts indicative of heightened inflammatory profiles in CAV lesions. Moreover, we identified protein and transcriptomic signatures distinguishing CAV lesions exhibiting low and high neointimal lesions. AOIs with low neointima showed increased markers for activated inflammatory infiltrates, endothelial cell activation transcripts, and gene modules involved in metalloproteinase activation and TP53 regulation of caspases. Inflammatory and apoptotic proteins correlated with inflammatory modules in low neointima AOIs. High neointima AOIs exhibited elevated TGFβ-regulated transcripts and modules enriched for platelet activation/aggregation. Proteins associated with growth factors/survival correlated with modules enriched for proliferation/repair in high neointima AOIs. Our findings reveal novel insight into immunological mechanisms mediating CAV pathogenesis.

This is an open access article under the CC BY-NC-ND license (http://creativecommons.org/licenses/by-nc-nd/4.0/).

*Corresponding author. Elaine F. Reed, University of California Los Angeles Department of Pathology and Laboratory Medicine Los Angeles, California, USA. ereed@mednet.ucla.edu (E.F. Reed).

Author contributions

J.N.-M. and E.F.R. designed research study. J.N.-M. and H.P. performed data analysis. R.A.S., G.A.F., and W.M.B. identified patient tissue, region selection, and grading. N.M.V., W.M.B., and R.L.F. contributed to the design of the study. J.N.-M. and E.F.R. wrote the manuscript. All authors read and approved the manuscript.

Declaration of competing interest

The authors of this manuscript have no conflicts of interest to disclose as described by the *American Journal of Transplantation*.

Appendix A. Supplementary data

Supplementary data to this article can be found online at https://doi.org/10.1016/j.ajt.2024.01.004.

Author Manuscript Author Manuscript Author Manuscript Author Manuscript

1. Introduction

Cardiac allograft vasculopathy (CAV) remains a major clinical challenge limiting long-term graft and patient survival following heart transplantation. Approximately 29% of heart transplant recipients develop CAV by 5 years and 47% by 10 years post-transplant.[1] CAV lesions are characterized by concentric intimal thickening of the vascular wall consisting of proliferating myofibroblast and inflammatory immune infiltrates.[2] Although both immunological and nonimmunological processes contribute to CAV pathogenesis, the exact mechanisms mediating disease pathogenesis remain unclear. Episodes of antibody-mediated rejection (AMR) in which donor-specific antibodies (DSAs) target human leukocyte antigens (HLAs) present on vascular endothelial cells (ECs) have been increasingly recognized as a major risk factor contributing to CAV.[3] Specifically, DSAs can activate EC intracellular signaling cascades, inducing EC proliferation, migration, and increased surface expression of adhesion molecules promoting monocyte and natural killer (NK) cell recruitment.[4–8] Moreover, DSAs can directly mediate EC injury by triggering activation of the classical complement cascade.[8] Recurring episodes of AMR contribute to chronic inflammation eliciting EC injury and apoptosis. $CD4^+$ and $CD8^+$ T cells activated by HLA alloantigen recognition are also commonly found in the adventitia and neointima of CAV-rejected hearts. Specifically, memory T helper 1 secreting proinflammatory cytokines such as IFN-γ and TNF-α can attract and activate $CD8^+$ cytotoxic T cells and NK cells.[2] T cells also secrete transforming growth factor-β (TGFβ), which significantly contributes to fibrosis and remodeling by upregulating collagen synthesis in smooth muscle cells (SMCs) and stimulating macrophage secretion of matrix metalloproteinases.[9] The process of endothelial-to-mesenchymal transition (EndoMT) remains another distinguishing characteristic contributing to CAV. EndoMT is a phenomenon in which ECs gradually lose EC markers and increase mesenchymal cell markers. A combination of inflammatory stimuli, low or disturbed shear flow, vascular stiffness (activating WNT/β-catenin), and metabolic dysregulation (eg, high glucose) can all cause EndoMT via different signaling pathways.[10]

Overall, numerous immunological mechanisms involving both innate and adaptive immune responses have been shown to contribute to the initiation and progression of neointimal development in CAV. Recent studies using endomyocardial biopsies (EMBs) have elucidated DSA- and/or AMR-specific bulk RNA signatures that contribute to CAV.[11–13] However, as CAV mainly affects large and small epicardial and intramyocardial arteries, EMBs may not exactly reflect the immune and/or vascular signatures contributing to neointima formation. Therefore, the proteomic and transcriptomic signatures revealing specific activated markers and regulatory pathways from CAV+DSA+ affected vessels as observed in rejected cardiac explants remains to be elucidated.

The goal of this study was to employ GeoMx digital spatial profiling (DSP) to conduct a patho-molecular and spatial analysis of CAV. Utilizing a multi-omics transcriptomics and proteomics approach, our results revealed transcripts and proteins consistently expressed in CAV lesions. Additionally, by comparing our transcriptomic data with that of healthy vessel controls, we pinpointed specific pathways and genes indicative of heightened inflammatory profiles in CAV lesions. Finally, a comparison between arterial regions with low and high

Author Manuscript Author Manuscript Author Manuscript Author Manuscript

neointimal scores uncovered inflammatory profiles in low neointima arteries, followed by profibrotic and reparative phenotypes in high neointima arteries. These findings contribute valuable insights into the mechanisms driving CAV pathogenesis, laying the groundwork for the identification of enhanced biomarkers for CAV diagnosis and treatment.

2. Methods

2.1. Study approval

The use of human cardiac rejected explants for this study was approved by the University of California, Los Angeles (UCLA) Institutional Review Board (IRB#18–001275). Formalin-fixed paraffin embedded tissue from rejected cardiac explants were obtained from the UCLA Translational Pathology Core Lab (TPCL).

2.2. Arterial vessel selection and pathological characteristics

A total of 22 geometric areas of interest (AOIs) were selected across 3 cardiac allograft explants from CAV+DSA+ patients (N = 3; 2 females patient ID [PID] 1, PID2 and 1 male PID3). These included 14 AOIs capturing the entire artery and 8 AOIs capturing a segment (or part) of the artery (particularly in the case of larger arteries where the maximal AOI surface area was reached). All 22 arterial AOIs included the neointima, media, and adventitia, encompassing all components of the vessel (Fig. 1A). Given the similarity in protein and transcript expression between the 14 AOIs (capturing entire arteries) and the 22 AOI dataset (Supplementary Fig. 1), we conducted downstream analysis using all 22 AOIs. Patient demographics, clinical information, and location of tissue section (eg, proximal posterior descending artery, right coronary artery, etc.) are summarized in Supplementary Table 1. The 22 AOIs included 10 vessels from PID1, 5 vessels from PID2, and 7 vessels from PID3. Hematoxylin and eosin (H&E) staining was used to score arteries based on the level of CAV progression/neointimal thickening by the pathologist. In total, 11 arteries were scored with ‘low’ neointima (+/− minimal and 1+ mild) and 11 with ‘high’ neointima (2+ moderate, 3+ significant, and 4+ very significant) (Supplementary Table 2). H&E images were captured using a Zeiss microscope and examined using ZEISS ZEN lite Software v3.3.

2.3. Targeted protein and whole transcriptome GeoMx digital spatial profiling (DSP)

Multiplex DSP of protein and RNA in fixed tissues was performed by NanoString Technologies (Seattle, WA) as part of the Technology Access Program as per Merritt et al[14] (Supplementary Methods 1.1).

2.4. Data normalization using NanoString’s GeoMx analysis suite

The GeoMx analysis suite was used for quality control and normalization of both protein and RNA datasets (Supplementary Methods 1.2).

Author Manuscript Author Manuscript Author Manuscript Author Manuscript

2.5. Weighted gene coexpression network analysis (WGCNA) analysis, gene regulatory networks (GRNs), and data deconvolution

WGCNA was used to define modules of coexpressed transcripts.[15] GRN analysis was performed using R package *SCENIC*.[16] RNA deconvolution was derived using SpatialDecon algorithm as previously described[17] (Supplementary Methods 1.3).

2.6. Multiplex-immunofluorescent staining

Multiplex-immunofluorescent staining of cardiac explants was performed by UCLA TPCL (Supplementary Methods 1.4).

2.7. Statistical analysis

Identification of differentially expressed proteins (DEPs), differentially expressed genes, and differentially expressed WGCNA modules between AOIs with low and high neointima were determined using a linear mixed-effects model, including PID as a random effect variable. Results were considered significant at $Log_2FC > 1$ and $P < .05$ for Figures 4B, C (Table 1) and $P < .05$ for Figure 4D. Statistical significance in Figure 2C was determined using Pearson correlation coefficient test, significant at $P < .05$. Results in Table 3 (and Supplementary Fig. 4) were determined using Spearman correlation (*$P < .05$, **$P < .01$, ***$P < .001$) in GraphPad Prism software v9.3.1.

3. Results

3.1. Arterial AOIs express protein markers related to immune cell activation and cell death.

Arterial AOIs from 3 CAV+DSA+ rejected cardiac explants (PID1–3; 2 females and 1 male; (Fig. 1A) were spatially profiled using a 73-protein panel (Supplementary Table 3). A total of 41 protein markers were similarly expressed across all 22 arterial AOIs (average signal to noise ratio [SNR] >1 in blue) (Fig. 1B). To assess variability in the structural make-up of the 22 captured AOIs, we additionally examined expressed proteins (average SNR > 1) in the 14 AOIs that encompassed entire arteries. A total of 44 protein markers were similarly expressed across the 14 AOIs (Supplementary Fig. 1A). Notably, all 41 proteins exhibited similar levels of expression (average SNR > 1) in both 22 AOI and 14 AOI datasets. Therefore, downstream analysis was conducted using all 22 AOIs. Specifically, all 22 AOIs expressed markers involved in immune cell activation and cytotoxicity (CD44, GZMB, and HLA-DR), apoptosis (cleaved caspase 9, BAD, and p53), and cell survival (BCL-XL). This was accompanied by the expression of $CD45^+$ immune infiltrates including macrophages (CD68), T cells (CD4 and CD8), NK cells (CD56), monocytes (CD14), and dendritic cells (CD11c), in order of expression. Phosphorylated proteins in the MAPK and PI3K/AKT signaling pathway (p44/42 MAPK ERK1/2, pan-AKT, and phospho-AKT1) were detected at moderate-to-low levels. Stimulator of interferons genes (STING) and TNFSF4/OX40L, a memory T cell survival-inducing ligand, also showed moderate-to-low levels of expression (Supplementary Table 4). Immunofluorescent staining validated the presence of low-to-moderately expressed proteins such as CD45RO, Ki-67, Tim-3 (approximate average SNR = 1) and CD127, p53, CD4 and CD8 (approx. average SNR = 2–4) (Supplementary Figure 2).

Author Manuscript Author Manuscript Author Manuscript Author Manuscript

Finally, protein correlation matrix analysis across all AOIs revealed significant associations between apoptotic and anti-apoptotic proteins (eg, BAD and BCL-XL), T cell markers (CD3 and CD8), and signaling cascades (phospho-AKT1 [S473] and pan-Ras) (Supplementary Fig. 3 and Supplementary Table 5).

3.2. Top transcripts in arteries encode for DSA-mediated immune responses and vascular remodeling

Transcriptomic analysis identified a total of 10 746 genes with an average SNR > 1 and coefficient of variation > 0.19 across all 22 arterial AOIs. A total of 74 transcripts had an average SNR > 10 (excluding ribosomal and ATP genes) (Fig. 2A). To assess for variability in the structural make-up of the 22 captured AOIs, we additionally examined gene expression levels in only the 14 AOIs encompassing entire arteries. Similar findings were observed, as 10 122 transcripts exhibited an average SNR > 1 and coefficient of variation > 0.19. Specifically, among the top 70 transcripts (average SNR > 10) identified in the 14 AOIs, there was almost complete overlap (65/70) with the top 74 transcripts observed in the 22 AOIs (Supplementary Fig. 1B). Given the similarity between both datasets, we proceeded with our analysis utilizing all 22 AOIs. The top 2 transcripts included *PTBP1*, a regulator of inflammation, and *ADAM15*, which mediates endothelial hyperpermeability during inflammation.[18,19] Immunoglobulin (IgG) transcripts (eg, *IGKC* and *IGHG1/2/3/4*) were also highly elevated. This was accompanied by the expression of HLA class I (*HLA-B*), IFN-γ inducible HLA class II molecules (eg, *HLA-DRB1* and *HLA-DRA*), and HLA class II chaperone transcripts (*CD74*).[20] AOIs also exhibited a relatively high expression of transcripts described in vascular remodeling, angiogenesis, platelet activation, cell proliferation, migration, and immune infiltration (*IGFBP7*, *TMSB4X*, *FLNA*, *TIMP1*, *MAZ*, *CRYAB*, *TMEM106C*).[21–26] Metascape gene enrichment analysis of the top 231 transcripts (average SNR > 5) revealed that AOIs were enriched in pathways relating to EC angiogenesis (‘*VEGFA-VEGFR2 signaling pathway*’), DSA activation (‘*immunoglobulin mediated immune responses*’), thrombosis (‘*platelet degranulation*’), and proinflammatory cytokines (‘*IL-18 signaling pathway*’) (Fig. 2B). Highly expressed transcripts were most likely attributed to fibroblasts, ECs, macrophages, and memory CD8 T cells, as these were the most prominent cell types by cellular abundance counts (Fig. 3A). Specifically, CD8 protein expression significantly correlated with CD8 memory abundance counts (and not CD8 naïve T cells), further suggesting the presence of memory T cells (Fig. 3B). Additionally, we identified CD45, CD8, CD56, CD20, CD127, and CD11c protein markers significantly correlated with RNA counterpart expression, validating the level of expression of these cell types in each AOI (Fig. 2C).

3.3. Vessels with CAV lesions exhibit elevated inflammatory profiles in comparison to vessels from healthy control myocardial tissues

To identify transcripts that were specific to or upregulated in CAV+DSA+ lesions, we compared transcripts with an average SNR > 1 to the dataset of Kulasinghe et al[27] containing GeoMx DSP transcriptomic data from 4 healthy control (HC) vessels of rapid autopsy myocardial tissues. A total of 1127 transcripts were shared between the 2 datasets. Unsupervised clustering revealed distinct gene expression profiles in CAV and HC vessels (Fig. 4A). Reactome pathway analysis of 193 genes with higher median

Author Manuscript Author Manuscript Author Manuscript Author Manuscript

expression in the CAV samples revealed heightened inflammatory pathways, including signaling by interleukins (IL-6), Toll-like receptor cascades (TLR4/7/8/9), MyD88 and MAPK cascades, chemokines, cyclin activation (G1), and antigen presentation (Fig. 4B). A total of 36 genes had a median fold change > 2 (CAV/HC) in CAV arteries compared to HC (Supplementary Table 6). Specifically, top genes mainly entailed those involved in antigen processing/presentation (*HLA-E* and *TAP1*), cancer cell proliferation and migration/ep ithelial-to-mesenchymal transition (EMT) (eg, *ITGA1*, *GPX1*, *PSMD7*, and *PPARGC1A*), fibroblast migration (*THBS4*), complement cascade regulation (*SERPING1*), and regulation of immune cell infiltration/inflammation (eg, *IFI6*, *GIMAP6*, *LGALS3*, *CCL14*, and *CCL21*).[28–40]

3.4. Arterial AOIs with low neointima exhibit higher inflammation and cell death while AOIs with high neointima exhibit remodeling and fibrotic profiles

Although all arteries were found to exhibit similar protein markers of both innate and adaptive immune infiltrates, we questioned whether the degree of inflammation varied between AOIs scored with a low (+/− minimal and 1+ mild) or high (2+ moderate, 3+ significant, and 4+ very significant) neointima (N = 11 AOIs for each condition). Unsupervised clustering of the 41 proteins (SNR > 1) illustrated that AOIs with low neointima clustered closer together and displayed higher protein expression (Fig. 5A). This was also observed when clustering AOIs for each individual patient (Supplementary Fig. 4). A total of 8 DEPs were increased in arteries with low neointima (Fig. 5B). These included markers involved in T cell clonal expansion/survival (TNFSF4/OX40L), memory T cells (CD45RO and CD127), checkpoint inhibitors (TIM-3), monocytes (CD14), regulators of PI3K/AKT signaling (INPP4B), MAPK signaling (pan-Ras), and proapoptotic proteins (p53) (Table 1). AOIs with low neointima also upregulated *VWF* (indicative of EC activation).[41] Meanwhile, AOIs with high neointima significantly increased TGFβ-regulated genes (*CSRP1* and *TAGLN)* and adipocyte differentiation factor (*ADIRF/APM2*) (Fig. 5C and Table 1).[42–44]

To further explore transcriptional differences between low and high neointima AOIs, we utilized WGCNA to define modules of coexpressed transcripts.[15] AOIs with low neointima-upregulated 3 modules (ME21, ME22, and ME118), 2 of which were enriched for '*Activation of matrix metalloproteinases*' and '*TP53 regulation of caspase activators and caspases*.' High neointima AOIs upregulated one module (ME50) enriched for pathways involved in '*Platelet activation, signaling and aggregation*' (Fig. 5D and Table 2). GRN analysis enabled the identification of key transcription factors correlating coexpression modules. Specifically, ME21 and ME118 highly correlated with inflammatory-driven transcription factors *SREBF2* and *NFATC1*, respectively.[45,46] Meanwhile, ME50 highly correlated with *NR2F2*, which promotes cell proliferation and TGFβ-dependent EMT (Fig. 5D and Table 2).[47]

Additionally, we identified that numerous protein markers encoding inflammatory infiltrates (eg, CD45, CD44, CD8, OX40L, GZMB) and apoptosis (p53 and BAD) highly correlated with coexpressing modules enriched for '*interferon gamma signaling*,' '*Toll-like receptor cascades*,' '*NFκB phosphorylation*,' and '*TP53 regulation of caspase activators and*

Author Manuscript Author Manuscript Author Manuscript Author Manuscript

caspases' (ME65, 77, 91, 118, 242, and 304) only in AOIs with low neointima. Alternatively, proteins associated with growth factor receptors (EGFR), regulators of cell growth/division (NF1), SMC markers (SMA), and cell survival proteins (BCL-XL) significantly correlated with modules enriched for '*MAPK1/MAPK3 signaling*,' '*signaling by FGFR*,' '*FGFR2 ligand binding and activation*,' and '*VEGFA-VEGFR2 pathway*' (ME161, 205, 206) only in AOIs with high neointima (Table 3 and Supplementary Fig. 5). Cellular deconvolution reinforced neointimal differences because AOIs with high neointima exhibited a significantly higher number of fibroblasts, while AOIs with low neointima contained a higher number of classical monocytes (Figure 3C).

4. Discussion

Herein, we utilized GeoMx DSP technology to examine both the protein and transcriptomic expression of arterial AOIs from HLA CAV+DSA+ rejected cardiac explants. Among the 22 arterial regions examined, we identified similarly expressed protein markers relating to innate and adaptive immune cells, cell activation, and cell death. Whole transcriptome analysis highlighted transcripts involved in DSA-mediated responses and vascular remodeling. Moreover, we confirmed the inflammatory profile of CAV lesions in comparison to HC vessels from rapid autopsy myocardial tissues. Finally, we demonstrated that AOIs with low neointima exhibit higher inflammatory and cell death profiles, while AOIs with high neointima exhibit lesions undergoing proliferation, migration, and EndoMT/fibrosis. Our findings provide new insights into the processes that may be driving CAV pathogenesis, opening avenues for further research and potential therapeutic interventions.

Macrophages and T cells have been found to accumulate within the neointima of human CAV affected vessels.[48,49] This is concordant with our study, as $CD68^+$ and $CD4/CD8^+$ markers were the top immune infiltrates in both protein and RNA cell abundance datasets. Monocyte recruitment may occur in the early phases of CAV, as we observed significantly higher protein expression of CD14 and classical monocytes counts in arteries with low neointima. HLA DSAs can rapidly increase intracellular calcium and endothelial presentation of P-selectin, which supports monocyte binding.[7,50] Notably, CD68 protein expression significantly correlated with module ME206 in high neointima AOIs. ME206 was enriched for pathways related to '*Fc gamma receptor dependent phagocytosis*,' indicative of polarized macrophage specific functions.[51]

Endothelial cell injury is a major hallmark of AMR and in the early phases of CAV. Specifically, high protein expression of $CD8^+$ T cells, CD44 activation marker, cleaved caspase 9, and GZMB together suggest cell-targeted injury via the perforin/granzyme apoptosis pathway by cytotoxic T cells. Human coronary arteries with advanced atherosclerosis and CAV lesions have been shown to exhibit high levels of GZMB localized within infiltrating leukocytes underlying the endothelium, in the deep intima, and in perivascular infiltrates in the adventitia.[52] GZMB-induced cell apoptosis can be enhanced by the proapoptotic protein BAD (BCL-2 associated agonist of cell death) or hindered by the antiapoptotic BCL-2 family protein, BCL-XL. These regulatory proteins share similar protein expression levels with GZMB and exhibit the highest significant correlation with each other. This is likely because activated BAD binds to and inhibits the antiapoptotic

Author Manuscript Author Manuscript Author Manuscript Author Manuscript

function of BCL-XL.[53] Expression of EC antiapoptotic proteins can be potentiated by antibody ligation of HLA class I and II molecules, which activate the PI3K/AKT pathway and upregulate BCL-2 and BCL-XL.[54] Hence, ECs may acquire antiapoptotic defense mechanisms that promote EndoMT via HLA outside-in signaling.

Arterial AOIs also showed high expression of transcripts associated with DSA-mediated responses including multiple IgGs, suggesting the presence of antibody-secreting cells such as B cells and/or plasma cells. Since CD20 protein expression across AOIs was relatively low (SNR = 1.21), it is likely that these IgG transcripts are encoded by mature plasma cells (which decrease CD20 expression). This was confirmed in a study by Chatterjee et al[55] in which the majority of the $CD138^+$ differentiated plasma cells around CAV affected coronary arteries from rejected explants secreted IgG. Moreover, microarray studies by Wehner et al[56] have shown a strong IgG transcriptome in CAV-rejected explants in contrast to atherosclerosis.

All arteries shared high expression for transcripts associated with EC and SMC activation, remodeling, angiogenesis, and platelet activation.[21–25] We compared transcripts with an average SNR > 5 to those identified in pathological AMR+DSA+ EMBs reported by Loupy et al[11] using microarray technology. Similarly, we detected the expression of IFN-γ inducible genes (HLA class II transcripts), and NK cell activation (*FCGR3A*). However, our results may not fully encompass the transcriptomic profile described by studies using EMBs due to anatomical differences within the heart. These differences have been emphasized in a mouse model of chronic AMR.[57]

Comparison of our transcriptomic data with those of HC myocardial vessels further validated the elevated inflammatory profiles of CAV arterial lesions. Specifically, CAV lesions exhibited a significant increase in TLR4/7/8/9, MyD88, MAPK, and IL-6 signaling compared to HC vessels. Studies by our group have emphasized the role of HLA DSA in activating EC outside-in intracellular signaling cascades such as TLR4/MyD88 and MAPK. Activation of these pathways induces EC proliferation and migration and promotes immune cell infiltration.[5–7,58,59] TLR4 expression has also been shown to be elevated in epicardial CAV lesions (compared to heart apical tissue) in a novel mouse model of chronic AMR.[57] Notably, increased IL-6 aligns with numerous studies that underscore its pleiotropic functions in mediating acute and chronic rejection.[60,61] CAV lesions also demonstrated an increased fold change expression in genes relating to antigen presentation, cell proliferation, migration, EMT, complement regulation, and inflammation. Precisely, *LGALS3* (Galectin-3) exhibited a 10-fold increase in CAV lesions compared to HC vessels. Galectin-3 regulates a variety of cellular processes such as growth, proliferation, and adhesion while also exerting immunomodulatory functions that impact both inflammation and fibrosis. High Galectin-3 levels are linked to heart failure and cardiac fibrosis, with recent research identifying Galectin-3 as an independent prognostic factor following heart transplantation.[62,63] Finally, *THBS4* (Thrombospondin-4) exhibited a 7-fold increase in CAV lesions. Thombospondin-4 is a main regulator of fibrosis/remodeling and can selectively promote fibroblast migration.[34,64] Together, these findings contribute valuable insights into the molecular aspects of vascular immunogenicity contributing to CAV progression.

Author Manuscript Author Manuscript Author Manuscript Author Manuscript

Multi-omics analysis between AOIs with low and high neointima revealed that low neointima AOIs exhibit higher inflammatory profiles consisting of lymphocyte and monocyte infiltrates, whereas high neointima AOIs contain higher proliferative and fibromuscular/mesenchymal tissue with lower inflammation. These observations are in accordance with the results of Huibers et al,[65] who identified 3 histopathological patterns of CAV characterized by inflammatory lesions and increased SMCs, followed by fibrotic lesions. AOIs with low neointima mainly exhibit features of burnt-out vasculitis (thickening of the vessel wall) or endothelialitis (cells beneath the endothelium). Based on the significantly higher memory T cell and cell death markers in low neointima AOIs, we speculate that T cells infiltrate subendothelial regions where they proliferate and mediate EC injury. The accumulation of T cells expressing perforin-containing granules in the subendothelial region of early CAV lesions has been previously reported.[66] OX40L (*TNFRSF4*) was the highest DEP between low and high neointima AOIs. OX40L (expressed on antigen-presenting cells, NK cells, activated CD4 T cells, ECs, and mast cells) binds to OX40+ antigen-activated T cells, stimulating T cell proliferation, clonal expansion/survival, and effector cytokine release.[67] Studies using mouse heart transplant models have highlighted the benefits of OX40L blockade in promoting graft survival by inducing Tregs.[68] AOIs with low neointima showing early vascular inflammation and cell death were supported by increased *VWF* and ME118 (enriched for TP53 activation of caspases), which significantly correlated with NFATC1, a regulator of cytotoxic $CD8^+$ T cells. AOIs with low neointima showed early vascular inflammation and cell death characteristics, supported by increased *VWF* and ME118 (enriched for TP53 activation of caspases). ME118 correlated significantly with *NFATC1*, a key regulator of cytotoxic $CD8^+$ T-cells[46].

Alternatively, AOIs with high neointima mainly demonstrated features of ongoing neointima expansion as seen by an increase in transcripts involved in myofibroblast differentiation (*CSRP1*), and remodeling (*TAGLN*).[42,43] AOIs with high neointima-upregulated pathways were related to '*Platelet activation, signaling and aggregation*' (ME50). DSA crosslinking to MHC I antigens induces Weibel-Palade bodies exocytosis of P-selectin and vWF, which can increase platelet and leukocyte infiltration, which aggravates vessel pathology.[7,50,69,70]

Finally, neointimal differences became more apparent, as the majority of markers encoding effector immune cell infiltrates significantly correlated with inflammatory comodules enriched for IFN-γ signaling, TLR cascades, and NFκB phosphorylation. Meanwhile, the majority of protein markers associated with cell growth factors and proliferation (eg, EGFR and NF1) correlated with profibrotic modules enriched for FGFR, FDFR2, and VEGFA-VEGFR2 signaling (Table 3). Antibody ligation of HLA I and HLA II molecules stimulates EC cell proliferation and migration via activation of PI3K/AKT, ERK, and mTOR signaling.[4,5,58] Moreover, anti-HLA I antibodies can mediate an increase in FGFR cell surface expression.[59] Together, these findings reinforce the notion that ECs and SMCs undergo active proliferative, migrative, and profibrotic signaling, contributing to vessel occlusion.

In summary, our findings highlight the heightened inflammatory profiles in CAV+DSA+ arterial regions and underscore the degree of heterogeneity among arterial vessels in rejected cardiac explants. Although our study reveals distinct profiles in CAV arterial

Author Manuscript Author Manuscript Author Manuscript Author Manuscript

lesions, there remain a few limitations to be addressed. First, DSP analysis represents data from a selected region rather than at the single-cell level. Ongoing studies are focused on identifying cell type-specific profiles. Furthermore, the geometric regions analyzed in this study encompassed various arterial components, including the neointima, media, and adventitia. Hence, our findings do not distinguish specific signatures associated with distinct compartments of the vessel. Further investigations employing more targeted region selection are needed to delineate these compartments. Second, despite encountering variability in patient characteristics, no significant correlations were found between patient age at transplant and neointima score nor with time posttransplant and neointima score. Finally, additional investigations utilizing DSA-negative explants, native ischemic hearts, and/or vessels with atherosclerosis would enhance the specificity of CAV lesion characteristics.

To our knowledge, this is the first spatial multi-omics study examining arterial vessels with varying degrees of neointima formation in CAV+DSA+ rejected cardiac allografts. Our findings further accentuate on the degree of vessel heterogeneity and inflammatory profiles not usually identified by pathology alone. We anticipate this newly generated dataset can serve as a resource for future high throughput or basic studies investigating the mechanisms of DSA-mediated injury and CAV development.

Supplementary Material

Refer to Web version on PubMed Central for supplementary material.

Acknowledgments

The authors thank the NanoString Technology Access Program (TAP) for this opportunity and UCLA TPCL for their resources. Finally, the authors thank the organ donors and their families for their generous gifts of life and knowledge.

Funding

This study was funded by the National Institute of Allergy and Infectious Diseases (NIAID) Grant R01AI135201 (E.F.R., R.L.F., N.M.V.), NIAID Grant R21AI156592 (E.F.R., R.L.F.), the National Institutes of Health (NIH) Ruth L. Kirschstein National Research Service Award (NRSA) T32HL069766 (J.N.-M.), and the UCLA Eugene V. Cota Robles Fellowship (J.N.-M.).

Data availability

The raw sequnce data will be publically available in Sequence Read Archive (SRA).

Abbreviations:

AMR	antibody-mediated rejection
AOI	area of interest
CAV	cardiac allograft vasculopathy
DSA	donor-specific antibodies
DEP	differentially expressed protein

Author Manuscript Author Manuscript Author Manuscript Author Manuscript

DSP	digital spatial profiling
EC	endothelial cell
EMB	endomyocardial biopsy
EMT	epithelial-to-mesenchymal transition
EndoMT	endothelial-to-mesenchymal transition
GRN	gene regulatory network
H&E	hematoxylin and eosin
HC	healthy control
HLA	human leukocyte antigen
IgG	immunoglobulin
NK	natural killer
PID	patient ID
SMC	smooth muscle cell
SNR	signal to noise ratio
TPCL	Translational Pathology Core Lab
UCLA	University of California, Los Angeles
WGCNA	weighted gene coexpression network analysis

References

1. Khush KK, Cherikh WS, Chambers DC, et al. The International Thoracic Organ Transplant Registry of the International Society for Heart and Lung Transplantation: Thirty-fifth Adult Heart Transplantation Report-2018; focus theme: multiorgan transplantation. J Heart Lung Transplant. 2018;37(10):1155–1168. 10.1016/j.healun.2018.07.022. [PubMed: 30293612]
2. Jansen MA, Otten HG, de Weger RA, Huibers MM. Immunological and fibrotic mechanisms in cardiac allograft vasculopathy. Transplantation. 2015;99(12):2467–2475. 10.1097/tp.0000000000000848. [PubMed: 26285017]
3. Colvin MM, Cook JL, Chang P, et al. Antibody-mediated rejection in cardiac transplantation: emerging knowledge in diagnosis and management: a scientific statement from the American Heart Association. Circulation. 2015;131(18):1608–1639. 10.1161/cir.0000000000000093. [PubMed: 25838326]
4. Zhang X, Rozengurt E, Reed EF. HLA class I molecules partner with integrin β4 to stimulate endothelial cell proliferation and migration. Sci Signal. 2010;3(149):ra85. 10.1126/scisignal.2001158. [PubMed: 21098729]
5. Jin YP, Valenzuela NM, Zhang X, Rozengurt E, Reed EF. HLA class II-triggered signaling cascades cause endothelial cell proliferation and migration: relevance to antibody-mediated transplant rejection. J Immunol 2018;200(7):2372–2390. 10.4049/jimmunol.1701259. [PubMed: 29475988]
6. Salehi S, Sosa RA, Jin YP, et al. Outside-in HLA class I signaling regulates ICAM-1 clustering and endothelial cell-monocyte interactions via mTOR in transplant antibody-mediated rejection. Am J Transplant. 2018;18(5):1096–1109. 10.1111/ajt.14544. [PubMed: 29045076]

Author Manuscript Author Manuscript Author Manuscript Author Manuscript

7. Jin YP, Nevarez-Mejia J, Terry AQ, et al. Cross-talk between HLA class I and TLR4 mediates P-selectin surface expression and monocyte capture to human endothelial cells. J Immunol 2022;209(7):1359–1369. 10.4049/jimmunol.2200284. [PubMed: 36165200]
8. Thomas KA, Valenzuela NM, Reed EF. The perfect storm: HLA antibodies, complement, FcγRs, and endothelium in transplant rejection. Trends Mol Med 2015;21(5):319–329. 10.1016/j.molmed.2015.02.004. [PubMed: 25801125]
9. Tellides G, Pober JS. Interferon-gamma axis in graft arteriosclerosis. Circ Res 2007;100(5):622–632. 10.1161/01.Res.0000258861.72279.29. [PubMed: 17363708]
10. Lu X, Gong J, Dennery PA, Yao H. Endothelial-to-mesenchymal transition: pathogenesis and therapeutic targets for chronic pulmonary and vascular diseases. Biochem Pharmacol 2019;168:100–107. 10.1016/j.bcp.2019.06.021. [PubMed: 31251941]
11. Loupy A, Duong Van Huyen JP, Hidalgo L, et al. Gene expression profiling for the identification and classification of antibody-mediated heart rejection. Circulation. 2017;135(10):917–935. 10.1161/circulationaha.116.022907. [PubMed: 28148598]
12. Halloran PF, Potena L, Van Huyen JD, et al. Building a tissue-based molecular diagnostic system in heart transplant rejection: the heart Molecular Microscope Diagnostic (MMDx) system. J Heart Lung Transplant. 2017;36(11):1192–1200. 10.1016/j.healun.2017.05.029. [PubMed: 28662985]
13. Mantell BS, Cordero H, See SB, et al. Transcriptomic heterogeneity of antibody mediated rejection after heart transplant with or without donor specific antibodies. J Heart Lung Transplant. 2021;40(11):1472–1480. 10.1016/j.healun.2021.06.012. [PubMed: 34420852]
14. Merritt CR, Ong GT, Church SE, et al. Multiplex digital spatial profiling of proteins and RNA in fixed tissue. Nat Biotechnol 2020;38(5):586–599. 10.1038/s41587-020-0472-9. [PubMed: 32393914]
15. Langfelder P, Horvath S. WGCNA: an R package for weighted correlation network analysis. BMC Bioinformatics. 2008;9:559. 10.1186/1471-2105-9-559. [PubMed: 19114008]
16. Aibar S, González-Blas CB, Moerman T, et al. SCENIC: single-cell regulatory network inference and clustering. Nat Methods. 2017;14(11): 1083–1086. 10.1038/nmeth.4463. [PubMed: 28991892]
17. Danaher P, Kim Y, Nelson B, et al. Advances in mixed cell deconvolution enable quantification of cell types in spatial transcriptomic data. Nat Commun 2022;13(1):385. 10.1038/s41467-022-28020-5. [PubMed: 35046414]
18. Sun C, Wu MH, Guo M, Day ML, Lee ES, Yuan SY. ADAM15 regulates endothelial permeability and neutrophil migration via Src/ERK1/2 signalling. Cardiovasc Res 2010;87(2):348–355. 10.1093/cvr/cvq060. [PubMed: 20189953]
19. Shu B, Zhou YX, Li H, Zhang RZ, He C, Yang X. The METTL3/MALAT1/PTBP1/USP8/TAK1 axis promotes pyroptosis and M1 polarization of macrophages and contributes to liver fibrosis. Cell Death Discov 2021; 7(1):368. 10.1038/s41420-021-00756-x. [PubMed: 34839365]
20. Su H, Na N, Zhang X, Zhao Y. The biological function and significance of CD74 in immune diseases. Inflamm Res 2017;66(3):209–216. 10.1007/s00011-016-0995-1. [PubMed: 27752708]
21. Lisowska A, Święcki P, Knapp M, et al. Insulin-like growth factor-binding protein 7 (IGFBP 7) as a new biomarker in coronary heart disease. Adv Med Sci 2019;64(1):195–201. 10.1016/j.advms.2018.08.017. [PubMed: 30769262]
22. Rossdeutsch A, Smart N, Dubé KN, Turner M, Riley PR. Essential role for thymosin β4 in regulating vascular smooth muscle cell development and vessel wall stability. Circ Res 2012;111(4):e89–e102. 10.1161/circresaha.111.259846. [PubMed: 22723298]
23. Bandaru S, Ala C, Zhou AX, Akyürek LM. Filamin A regulates cardiovascular remodeling. Int J Mol Sci 2021;22(12):6555. 10.3390/ijms22126555. [PubMed: 34207234]
24. Barton PJ, Birks EJ, Felkin LE, Cullen ME, Koban MU, Yacoub MH. Increased expression of extracellular matrix regulators TIMP1 and MMP1 in deteriorating heart failure. J Heart Lung Transplant. 2003; 22(7):738–744. 10.1016/s1053-2498(02)00557-0. [PubMed: 12873541]
25. Smits M, Wurdinger T, van het Hof B, et al. Myc-associated zinc finger protein (MAZ) is regulated by miR-125b and mediates VEGF-induced angiogenesis in glioblastoma. FASEB J 2012;26(6):2639–2647. 10.1096/fj.11-202820. [PubMed: 22415301]

Author Manuscript Author Manuscript Author Manuscript Author Manuscript

26. Zhang J, Liu J, Wu J, Li W, Chen Z, Yang L. Progression of the role of CRYAB in signaling pathways and cancers. Onco Targets Ther 2019; 12:4129–4139. 10.2147/ott.S201799. [PubMed: 31239701]
27. Kulasinghe A, Liu N, Tan CW, et al. Transcriptomic profiling of cardiac tissues from SARS-CoV-2 patients identifies DNA damage. Immunology. 2023;168(3):403–419. 10.1111/imm.13577. [PubMed: 36107637]
28. Zhao Y, Wang H, Zhou J, Shao Q. Glutathione peroxidase GPX1 and its dichotomous roles in cancer. Cancers (Basel). 2022;14(10):2560. 10.3390/cancers14102560. [PubMed: 35626163]
29. Zhang Q, Xiong L, Wei T, et al. Hypoxia-responsive PPARGC1A/BAMBI/ACSL5 axis promotes progression and resistance to lenvatinib in hepatocellular carcinoma. Oncogene 2023;42(19):1509–1523. 10.1038/s41388-023-02665-y. [PubMed: 36932115]
30. Yao Y, Du Jiang P, Chao BN, et al. GIMAP6 regulates autophagy, immune competence, and inflammation in mice and humans. J Exp Med 2022;219(6):e20201405. 10.1084/jem.20201405. [PubMed: 35551368]
31. Wang J, Liu R, Mo H, Xiao X, Xu Q, Zhao W. Deubiquitinase PSMD7 promotes the proliferation, invasion, and cisplatin resistance of gastric cancer cells by stabilizing RAD23B. Int J Biol Sci 2021;17(13): 3331–3342. 10.7150/ijbs.61128. [PubMed: 34512150]
32. Tabassum A, Samdani MN, Dhali TC, et al. Transporter associated with antigen processing 1 (TAP1) expression and prognostic analysis in breast, lung, liver, and ovarian cancer. J Mol Med (Berl). 2021;99(9): 1293–1309. 10.1007/s00109-021-02088-w. [PubMed: 34047812]
33. Liu J, Chen H, Qiao G, et al. PLEK2 and IFI6, representing mesenchymal and immune-suppressive microenvironment, predicts resistance to neoadjuvant immunotherapy in esophageal squamous cell carcinoma. Cancer Immunol Immunother 2023;72(4):881–893. 10.1007/s00262-022-03288-0. [PubMed: 36121452]
34. Klaas M, Mäemets-Allas K, Heinmäe E, et al. Thrombospondin-4 is a soluble dermal inflammatory signal that selectively promotes fibroblast migration and keratinocyte proliferation for skin regeneration and wound healing. Front Cell Dev Biol 2021;9:745637. 10.3389/fcell.2021.745637. [PubMed: 34631719]
35. Kim SJ, Karamooz E. MR1- and HLA-E-dependent antigen presentation of Mycobacterium tuberculosis. Int J Mol Sci 2022;23(22):14412. 10.3390/ijms232214412. [PubMed: 36430890]
36. Hara A, Niwa M, Kanayama T, et al. Galectin-3: a potential prognostic and diagnostic marker for heart disease and detection of early stage pathology. Biomolecules. 2020;10(9):1277. 10.3390/biom10091277. [PubMed: 32899694]
37. Gu Y, Li X, Bi Y, et al. CCL14 is a prognostic biomarker and correlates with immune infiltrates in hepatocellular carcinoma. Aging (Albany NY). 2020;12(1):784–807. 10.18632/aging.102656. [PubMed: 31927532]
38. Gharibi A, La Kim S, Molnar J, et al. ITGA1 is a pre-malignant biomarker that promotes therapy resistance and metastatic potential in pancreatic cancer. Sci Rep 2017;7(1):10060. 10.1038/s41598-017-09946-z. [PubMed: 28855593]
39. Chen Y, Shao Z, Jiang E, et al. CCL21/CCR7 interaction promotes EMT and enhances the stemness of OSCC via a JAK2/STAT3 signaling pathway. J Cell Physiol 2020;235(9):5995–6009. 10.1002/jcp.29525. [PubMed: 32017846]
40. Allswede DM, Zheutlin AB, Chung Y, et al. Complement gene expression correlates with superior frontal cortical thickness in humans. Neuropsychopharmacology. 2018;43(3):525–533. 10.1038/npp.2017.164. [PubMed: 28758643]
41. Ruggeri ZM. The role of von Willebrand factor in thrombus formation. Thromb Res 2007;120(suppl 1):S5–S9. 10.1016/j.thromres.2007.03.011. [PubMed: 17493665]
42. Järvinen PM, Myllärniemi M, Liu H, et al. Cysteine-rich protein 1 is regulated by transforming growth factor-β1 and expressed in lung fibrosis. J Cell Physiol 2012;227(6):2605–2612. 10.1002/jcp.23000. [PubMed: 21882188]
43. Elsafadi M, Manikandan M, Dawud RA, et al. Transgelin is a TGFβ-inducible gene that regulates osteoblastic and adipogenic differentiation of human skeletal stem cells through actin cytoskeleston organization. Cell Death Dis 2016;7(8):e2321. 10.1038/cddis.2016.196. [PubMed: 27490926]

Author Manuscript Author Manuscript Author Manuscript Author Manuscript

44. Scott BJ, Qutob S, Liu QY, Ng CE. APM2 is a novel mediator of cisplatin resistance in a variety of cancer cell types regardless of p53 or MMR status. Int J Cancer. 2009;125(5):1193–1204. 10.1002/ijc.24465. [PubMed: 19444912]
45. Dong G, Huang X, Wu L, Jiang S, Tan Q, Chen S. SREBF2 triggers endoplasmic reticulum stress and Bax dysregulation to promote lipopolysaccharide-induced endothelial cell injury. Cell Biol Toxicol 2022;38(1):185–201. 10.1007/s10565-021-09593-1. [PubMed: 33677747]
46. Klein-Hessling S, Muhammad K, Klein M, et al. NFATc1 controls the cytotoxicity of $CD8^+$ T cells. Nat Commun 2017;8(1):511. 10.1038/s41467-017-00612-6. [PubMed: 28894104]
47. Wang H, Nie L, Wu L, Liu Q, Guo X. NR2F2 inhibits Smad7 expression and promotes TGF-β-dependent epithelial-mesenchymal transition of CRC via transactivation of miR-21. Biochem Biophys Res Commun 2017;485(1):181–188. 10.1016/j.bbrc.2017.02.049. [PubMed: 28192117]
48. Berry GJ, Burke MM, Andersen C, et al. The 2013 International Society for Heart and Lung Transplantation Working Formulation for the standardization of nomenclature in the pathologic diagnosis of antibody-mediated rejection in heart transplantation. J Heart Lung Transplant. 2013;32(12):1147–1162. 10.1016/j.healun.2013.08.011. [PubMed: 24263017]
49. Lu WH, Palatnik K, Fishbein GA, et al. Diverse morphologic manifestations of cardiac allograft vasculopathy: a pathologic study of 64 allograft hearts. J Heart Lung Transplant. 2011;30(9):1044–1050. 10.1016/j.healun.2011.04.008. [PubMed: 21640617]
50. Valenzuela NM, Hong L, Shen XD, et al. Blockade of p-selectin is sufficient to reduce MHC I antibody-elicited monocyte recruitment in vitro and in vivo. Am J Transplant. 2013;13(2):299–311. 10.1111/ajt.12016. [PubMed: 23279566]
51. Wei X, Valenzuela NM, Rossetti M, et al. Antibody-induced vascular inflammation skews infiltrating macrophages to a novel remodeling phenotype in a model of transplant rejection. Am J Transplant. 2020; 20(10):2686–2702. 10.1111/ajt.15934. [PubMed: 32320528]
52. Choy JC, McDonald PC, Suarez AC, et al. Granzyme B in atherosclerosis and transplant vascular disease: association with cell death and atherosclerotic disease severity. Mod Pathol 2003;16(5):460–470. 10.1097/01.Mp.0000067424.12280.Bc. [PubMed: 12748253]
53. Adachi M, Imai K. The proapoptotic BH3-only protein BAD transduces cell death signals independently of its interaction with Bcl-2. Cell Death Differ 2002;9(11):1240–1247. 10.1038/sj.cdd.4401097. [PubMed: 12404123]
54. Jin YP, Fishbein MC, Said JW, et al. Anti-HLA class I antibody-mediated activation of the PI3K/Akt signaling pathway and induction of Bcl-2 and Bcl-xL expression in endothelial cells. Hum Immunol 2004;65(4): 291–302. 10.1016/j.humimm.2004.01.002. [PubMed: 15120184]
55. Chatterjee D, Moore C, Gao B, et al. Prevalence of polyreactive innate clones among graft–infiltrating B cells in human cardiac allograft vasculopathy. J Heart Lung Transplant. 2018;37(3):385–393. 10.1016/j.healun.2017.09.011. [PubMed: 29055600]
56. Wehner J, Morrell CN, Reynolds T, Rodriguez ER, Baldwin 3rd WM. Antibody and complement in transplant vasculopathy. Circ Res 2007;100(2):191–203. 10.1161/01.Res.0000255032.33661.88. [PubMed: 17272820]
57. Tsuda H, Dvorina N, Keslar KS, et al. Molecular signature of antibody-mediated chronic vasculopathy in heart allografts in a novel mouse model. Am J Pathol 2022;192(7):1053–1065. 10.1016/j.ajpath.2022.04.003. [PubMed: 35490714]
58. Jin YP, Valenzuela NM, Ziegler ME, Rozengurt E, Reed EF. Everolimus inhibits anti-HLA I antibody-mediated endothelial cell signaling, migration and proliferation more potently than sirolimus. Am J Transplant. 2014;14(4):806–819. 10.1111/ajt.12669. [PubMed: 24580843]
59. Jin YP, Singh RP, Du ZY, Rajasekaran AK, Rozengurt E, Reed EF. Ligation of HLA class I molecules on endothelial cells induces phosphorylation of Src, paxillin, and focal adhesion kinase in an actin-dependent manner. J Immunol 2002;168(11):5415–5423. 10.4049/jimmunol.168.11.5415. [PubMed: 12023334]
60. Miller CL, Madsen JC. IL-6 directed therapy in transplantation. Curr Transplant Rep 2021;8(3):191–204. 10.1007/s40472-021-00331-4. [PubMed: 34099967]
61. Miller CL, Madsen JC. Targeting IL-6 to prevent cardiac allograft rejection. Am J Transplant. 2022;22(suppl 4):12–17. 10.1111/ajt.17206.

Author Manuscript Author Manuscript Author Manuscript Author Manuscript

62. Blanda V, Bracale UM, Di Taranto MD, Fortunato G. Galectin-3 in cardiovascular diseases. Int J Mol Sci 2020;21(23):9232. 10.3390/ijms21239232. [PubMed: 33287402]

63. Franeková J, Hošková L, Jabor A. Galectin-3 as an independent prognostic factor after heart transplantation. Clin Transplant. 2022;36(5): e14592. 10.1111/ctr.14592. [PubMed: 35029311]

64. Frolova EG, Sopko N, Blech L, et al. Thrombospondin-4 regulates fibrosis and remodeling of the myocardium in response to pressure overload. FASEB J 2012;26(6):2363–2373. 10.1096/fj.11-190728. [PubMed: 22362893]

65. Huibers MM, Vink A, Kaldeway J, et al. Distinct phenotypes of cardiac allograft vasculopathy after heart transplantation: a histopathological study. Atherosclerosis. 2014;236(2):353–359. 10.1016/j.atherosclerosis.2014.07.016. [PubMed: 25128973]

66. Hruban RH, Beschorner WE, Baumgartner WA, et al. Accelerated arteriosclerosis in heart transplant recipients is associated with a T-lymphocyte-mediated endothelialitis. Am J Pathol 1990;137(4):871–882. [PubMed: 1699422]

67. Fu Y, Lin Q, Zhang Z, Zhang L. Therapeutic strategies for the costimulatory molecule OX40 in T-cell-mediated immunity. Acta Pharm Sin B 2020;10(3):414–433. 10.1016/j.apsb.2019.08.010. [PubMed: 32140389]

68. Tkachev V, Furlan SN, Watkins B, et al. Combined OX40L and mTOR blockade controls effector T cell activation while preserving Treg reconstitution after transplant. Sci Transl Med 2017;9(408):eaan3085. 10.1126/scitranslmed.aan3085. [PubMed: 28931653]

69. Morrell CN, Murata K, Swaim AM, et al. In vivo platelet-endothelial cell interactions in response to major histocompatibility complex alloantibody. Circ Res 2008;102(7):777–785. 10.1161/circresaha.107.170332. [PubMed: 18296616]

70. Valenzuela NM, Mulder A, Reed EF. HLA class I antibodies trigger increased adherence of monocytes to endothelial cells by eliciting an increase in endothelial P-selectin and, depending on subclass, by engaging FcγRs. J Immunol 2013;190(12):6635–6650. 10.4049/jimmunol.1201434. [PubMed: 23690477]

Author Manuscript Author Manuscript Author Manuscript Author Manuscript

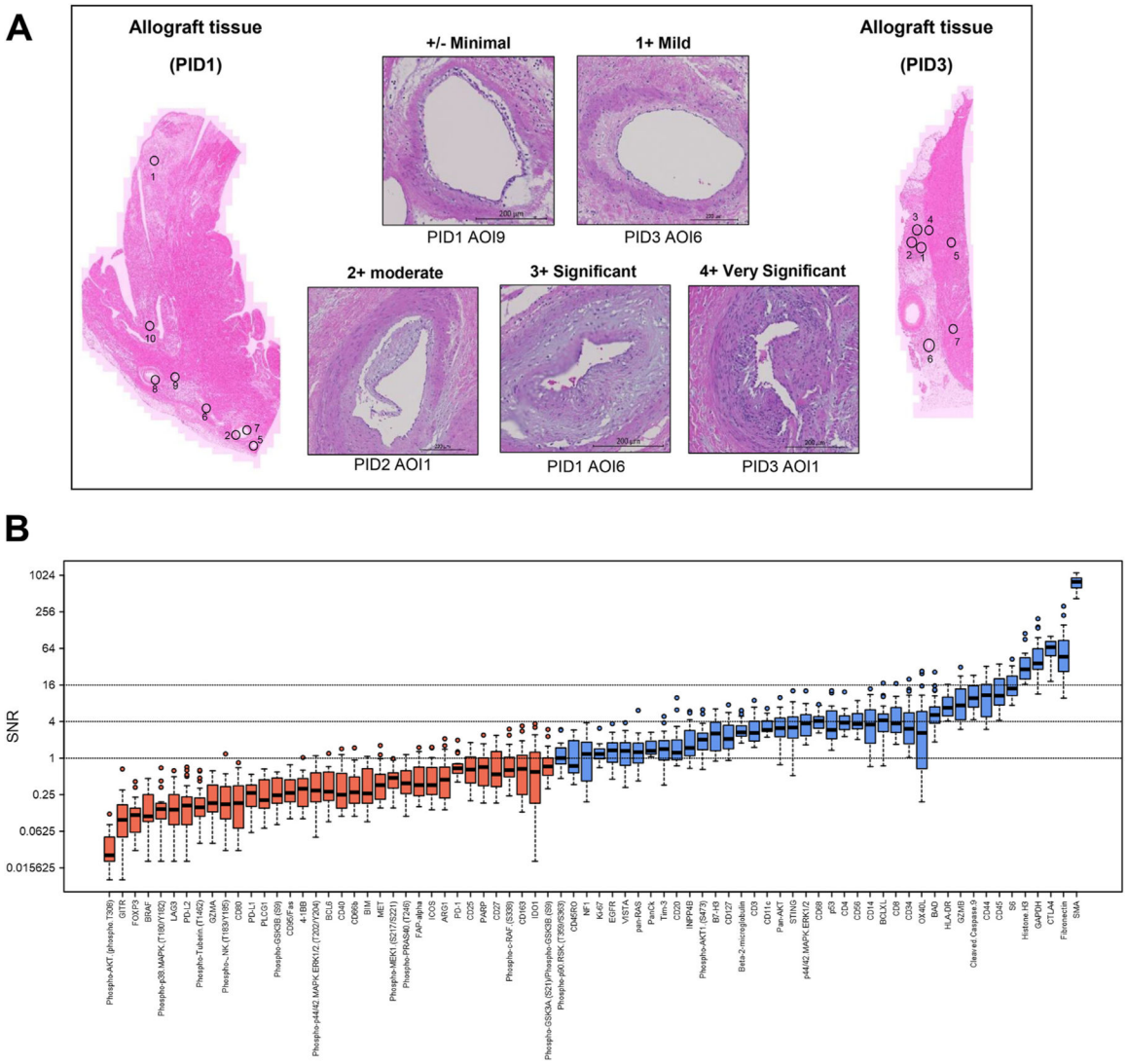

Figure 1.

Arterial regions from cardiac allograft vasculopathy (CAV) rejected grafts exhibit varying degrees of neointimal thickening and express 41 protein markers. (A) A total of 22 arterial areas of interest (AOIs) from CAV+DSA+ patients (PID1–3; 2 females and 1 male) were subjected to protein and RNA digital spatial profiling. In total, 11 AOIs were scored with 'low' neointima (+/− minimal and 1+ mild) and 11 with 'high' neointima (2+ moderate, 3+ significant, and 4+ very significant) by hematoxylin and eosin staining (scale bar = 200μm). (B) Protein profiling identified a total of 41 protein markers which were similarly expressed across all 22 AOIs (average signal to noise ratio [SNR] >1 in blue). Protein data was normalized to the average of negative IgG controls and reported as SNR. Proteins with an average SNR <1 (in red) were considered not expressed. Data ranked by average values. PID, patient ID.

Author Manuscript Author Manuscript Author Manuscript Author Manuscript

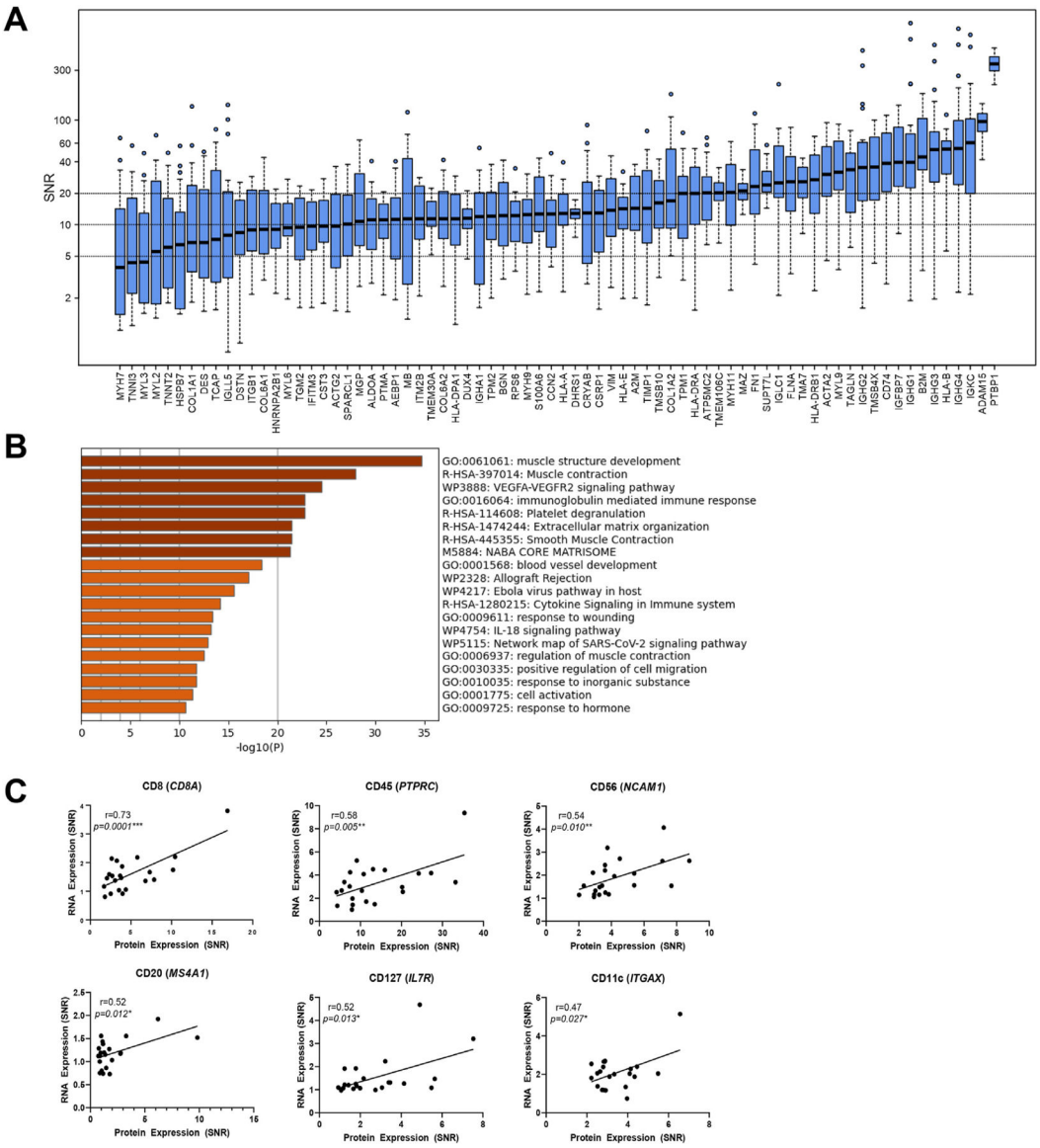

Figure 2.

Top transcripts in arterial AOIs encode for DSA-mediated immune responses and vascular remodeling. (A) Expression levels of the top 74 transcripts (average SNR > 10) ranked by median values (excluding ribosomal and ATP transcripts). Whole genome RNA data was normalized to the average (+2 SD) of internal negative controls (NegProbe-WTX) and is reported as an SNR. (B) Pathway enrichment analysis of the top 231 transcripts (with average SNR > 5) using Metascape. (C) The protein expression of CD8, CD45, CD56, CD20, CD127, and CD11c exhibited a significantly positive correlation with RNA counterpart expression. Statistical significance was determined using Pearson correlation test (* P <.05, ** P <.01, *** P < .001). AOI, area of interest; SD, standard deviation; SNR, signal to noise ratio.

Author Manuscript Author Manuscript Author Manuscript Author Manuscript

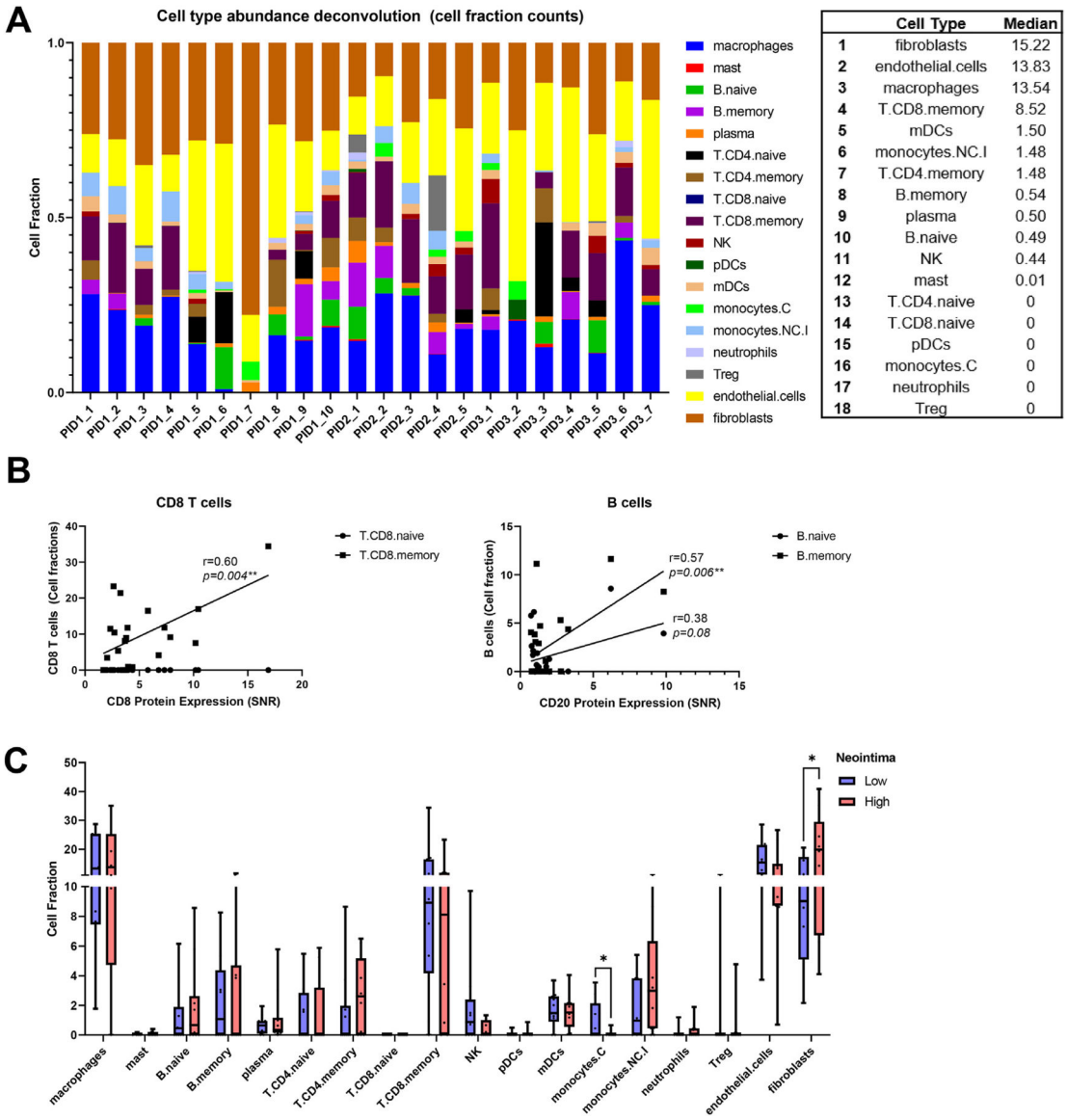

	Cell Type	Median
1	fibroblasts	15.22
2	endothelial.cells	13.83
3	macrophages	13.54
4	T.CD8.memory	8.52
5	mDCs	1.50
6	monocytes.NC.I	1.48
7	T.CD4.memory	1.48
8	B.memory	0.54
9	plasma	0.50
10	B.naive	0.49
11	NK	0.44
12	mast	0.01
13	T.CD4.naive	0
14	T.CD8.naive	0
15	pDCs	0
16	monocytes.C	0
17	neutrophils	0
18	Treg	0

Figure 3.

Fibroblasts, endothelial cells, macrophages, and memory CD8 T cells showed the highest expression across all arterial AOIs. (A) RNA data deconvolution of cell type abundance estimates across all arterial AOIs was derived using SpatialDecon algorithm. Fibroblasts, ECs, macrophages, and memory CD8 T cells were the most prominent cell types across AOIs. (B) Deconvolution cell fraction counts for $CD8^+$ memory T cells and CD20 memory B cells significantly correlated with protein expression counterparts (SNR counts) (determined by Pearson correlation coefficient test (**$P < .01$). (C) Cell fraction counts for each cell type between low and high neointima AOIs. Classical monocytes were significantly elevated in AOIs with low neointima while fibroblast cell fractions were higher in AOIs with high neointima. Significance was determined by non-paired Student *t* test (*$P < .05$). AOI, area of interest; EC, endothelial cell; SNR, signal to noise ratio.

Author Manuscript Author Manuscript Author Manuscript Author Manuscript

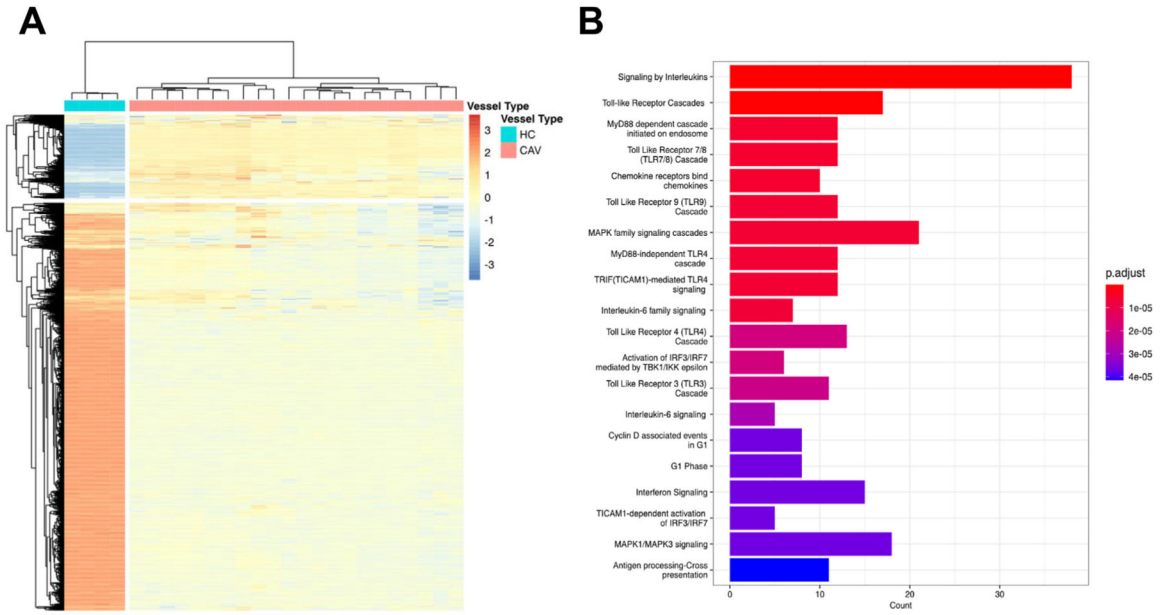

Figure 4.

Cardiac allograft vasculopathy (CAV) arterial lesions exhibit higher inflammatory profiles compared to vessels from myocardial healthy controls (HCs). (A) Unsupervised clustering of z-score normalized expression of 1127 genes shared between CAV lesions (red) and myocardial HC vessels (blue). (B) Reactome pathway analysis of the 193 genes upregulated in the CAV lesions reveals increased inflammatory profiles.

Author Manuscript Author Manuscript Author Manuscript Author Manuscript

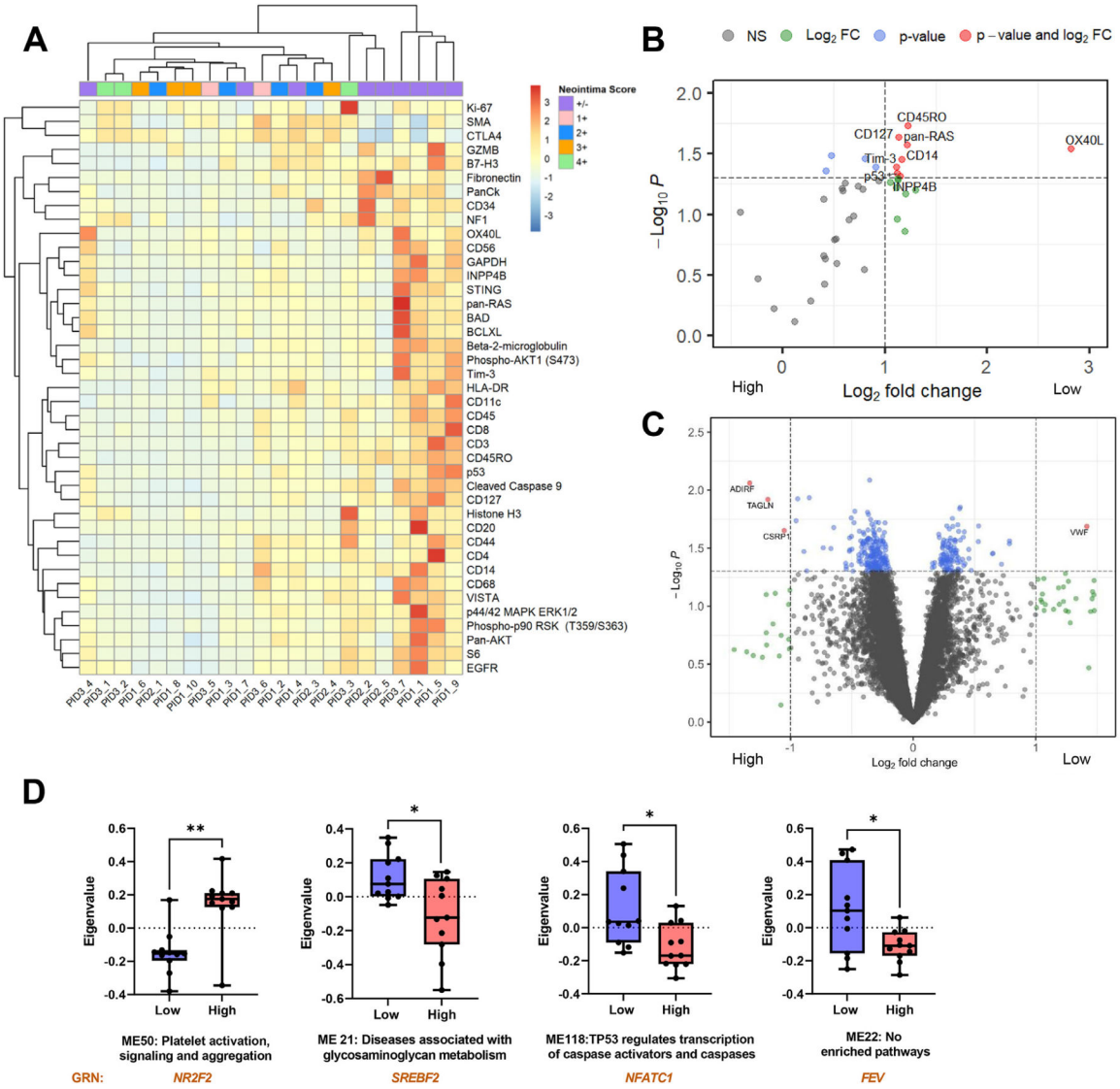

Figure 5.

Arterial AOIs containing high and low neointima exhibit differences in protein and RNA expression. (A) Unsupervised clustering of the 41 expressed proteins (average SNR >1) across all 22 arterial AOIs. (B) Differentially expressed proteins (in red dots) between AOIs with low and high neointima. (C) Differentially expressed genes between AOIs with low and high neointima (in red dots). (D) Weighted gene coexpression network analysis was used to generate gene modules (ME) of coexpressed genes. Expression of each module is represented by eigengene values (Eigen-value). Module names were defined by Reactome pathway enrichment analysis. Arterial AOIs with low neointima increased ME21, ME22, and ME118 while AOIs with high neointima increased ME50. The highest positively correlated gene regulatory network (GNR) for each module is included below (orange text). Statistical significance for volcano plots ($Log_2FC > 1$ and $P < .05$) and for comparing modules (Eigenvalues) was determined using linear mixed-effects model (including PID as

random effects) using in R software (*P <.05, **P <.01). AOI, area of interest; FC, fold change; PID, patient ID.

Author Manuscript Author Manuscript Author Manuscript Author Manuscript

Author Manuscript

Author Manuscript

Author Manuscript

Author Manuscript

Table 1

Differentially expressed proteins and differentially expressed genes between low and high neointima areas of interest.

	Protein	**Log_2FC**	***P***
1	OX40L	2.82	*.029*
2	CD45RO	1.23	*.019*
3	pan-RAS	1.22	*.027*
4	CD14	1.17	*.035*
5	INPP4B	1.15	*.049*
6	CD127	1.14	*.023*
7	p53	1.12	*.046*
8	Tim-3	1.11	*.041*
	Gene	**Log_2FC**	***P***
1	*VWF*	1.42	*.021*
2	*CSRP1*	−1.05	*.022*
3	*TAGLN*	−1.18	*.012*
4	*ADIRF*	−1.33	*.009*

FC, fold change.

Author Manuscript Author Manuscript Author Manuscript Author Manuscript

Table 2

Differentially expressed modules between low and high neointima AOIs and highest positively correlated GRN ($P < .5$).

Module name	Total genes	Representative genes[a]	Enriched pathway[b] (genes in enriched pathways)	GRN	Neointima
ME21	8	ASCL5, CLDN7, CLEC4F, CTRB1, GPC5, NECTIN4, NKAIN4, TMEM97	Cell-cell junction organization (NECTIN4, CLDN7); activation of matrix metalloproteinases (CTRB1); diseases associated with glycosaminoglycan metabolism (GPC5)	SREBF2	↑Low
ME22	7	ABCC8, HOXD12, RXFP2, SHOC1, WRAP73, ZNF283, ZNF649	No enriched pathway(s)	FEV	↑Low
ME50	11	GRAMD1C, ITIH3, ITIH4, LURAP1L, MRPS14, PAWR, RAD51B, REXO5, RHOB, SMTN, ZDHHC11	Platelet activation, signaling, and aggregation (RHOB/ITIH4/ITIH3); diseases of DNA repair (RAD51B)	NR2F2	↑High
ME118	15	ACSM3, ARHGAP28, CITED1, CNPY1, EFCAB8, F9, ITGAX, KCNJ13, KCP, MMP26, MTNR1A, OR1Q1, PRICKLE4, SEPTIN3, SLC25A15, SMG9, TMEM14A, TMEM269, TP63, TRAIP	TP53 regulates transcription of caspase activators and caspases (TP63); activation of the TFAP2 (AP-2) family of transcription factors (CITED1); γ-carboxylation of protein precursors (F9); urea cycle (SLC25A15)	NFATC1	↑Low

AOI, area of interest; GRN, gene regulatory network.

[a]Genes with expression pattern best representative of combined module of coexpressed genes

[b]Enrichment pathway defined by Reactome and (genes in enriched pathways)

Author Manuscript Author Manuscript Author Manuscript Author Manuscript

Table 3

Highly correlated proteins with WGCNA modules between low and high neointima AOIs.

Module	Protein	Low neointima AOIs			High neointima AOIs			Representative genes[a]	Enriched pathway[b] (genes in enriched pathway)
		r	*P*		r	*P*			
ME65	B7-H3	.78	**	*.006*	−.08	*ns*	*.818*	CD80, GGACT, OR52M1, PALD1, PTK7, SMIM41	Costimulation by the CD28 family (CD80)
	GZMB	.76	**	*.009*	−.34	*ns*	*.313*		
	Fibronectin	.75	*	*.011*	−.51	*ns*	*.114*		
ME77	Ki-67	.71	*	*.018*	.73	*	*.014*	ABCA6, APOC3, ATE1, CC2D1A, CD163, CDKL3, CHI3L1, DSTYK, H4C9, HK3, HLA-DQA1, HLA-DQB1, IFT27, ITGAX, KLHDC4, MAP3K8, PCYOX1L, PFKFB3, PLA1A, PLTP, TFRC, TNC, TRAPPC2L, TREML2, TRIM14, ZC3H12A, ZNF394, ZNF461	Costimulation by the CD28 family (HLA-DQB1, MAP3K8, HLA-DQA1); interferon-γ signaling (HLA-DQB1/HLA-DQA1, TRIM14); HDL remodeling (PLTP, APOC3)
	CD8	.68	*	*.025*	.35	*ns*	*.286*		
	CD68	.67	*	*.028*	.12	*ns*	*.735*		
	CD44	.65	*	*.037*	.14	*ns*	*.694*		
	CD45	.64	*	*.04*	.28	*ns*	*.402*		
ME91	GZMB	.74	*	*.013*	−.07	*ns*	*.839*	B3GNT8, IRAK2, ITM2A, KNOP1, NUDCD2, PMEL, SCN3A, SP140, ZBTB18, ZDHHC17	Toll-like receptor cascades (IRAK2); *O*-linked glycosylation of mucins (B3GNT8); TAK1 activates NFκB by phosphorylation and activation of IKKs complex (IRAK2); L1CAM interactions (SCN3A)
	p53	.65	*	*.037*	.61	*ns*	*.052*		
ME118	GZMB	.67	*	*.028*	−.75	**	*.010*	ACSM3, ARHGAP28, CITED1, CNPY1, EFCAB8, F9, ITGAX, KCNJ13, KCP, MMP26, MTNR1A, OR1Q1, PRICKLE4, SEPTIN3, SLC25A15, SMG9, TMEM14A, TMEM269, TP63, TRAIP	TP53 regulates transcription of caspase activators and caspases (TP63); activation of the TFAP2 (AP-2) family of transcription factors (CITED1); γ-carboxylation of protein precursors (F9); urea cycle (SLC25A15)
	Fibronectin	.62	*	*.048*	−.04	*ns*	*.924*		
ME242	CD56	.80	**	*.005*	−.03	*ns*	*.946*	CNMD, DTYMK, GORAB, METTL21A, NOL7, STUB1, TRAF6, ZBTB4, ZNF772	TGFβ receptor signaling activates SMADs (STUB1); TAK1 activates NFκB by phosphorylation and activation of IKKs complex (TRAF6); protein methylation (METTL21A)
	OX40L	.80	**	*.005*	−.2	*ns*	*.557*		
	BAD	.62	*	*.048*	−.35	*ns*	*.299*		
ME304	Ki-67	.79	**	*.006*	.12	*ns*	*.735*	BRI3BP, C9, CRYBB2, DZIP1, GALNT13, GBP3, ITGAX, LUZP2, NQO2, OAS1, SLC25A32, USHBP1	Interferon-γ signaling (OAS1, GBP3)
	HLA-DR	.73	*	*.010*	.59	*ns*	*.056*		
	Tim-3	.68	*	*.025*	.38	*ns*	*.244*		
ME161	NF1	−.20	*ns*	*.562*	.86	**	*.001*	CASP3, CORT, DCAF8L2, FRS3, ISM1, NSRP1, PITHD1, SFRP5, SHC3, WDR5B	MAPK1/MAPK3 signaling (FRS3/SHC3); signaling by FGFR (FRS3); apoptotic factor-mediated response (CASP3)
	Fibronectin	−.54	*ns*	*.094*	.65	*	*.034*		
	SMA	.09	*ns*	*.796*	.63	*	*.044*		
ME205	EGFR	.09	*ns*	*.796*	.8	**	*.005*	ASCL3, FGFBP2, KIF1A, OR2G3, OTUD1	FGFR2b ligand binding and activation (FGFBP2); COPI-dependent Golgi-to-ER retrograde traffic (KIF1A)
	STING	.17	*ns*	*.615*	.78	**	*.006*		
	Histone H3	−.25	*ns*	*.468*	.69	*	*.023*		

Author Manuscript Author Manuscript Author Manuscript Author Manuscript

Module	Protein	Low neointima AOIs			High neointima AOIs			Representative genes[a]	Enriched pathway[b] (genes in enriched pathway)
		r	*P*		r	*P*			
ME206	CD11c	.25	*ns*	*.451*	.79	**	*.006*	BARHL1, C19orf71, ELMO2, FSCB, SHCBP1, ULK4	PTK6 regulates RHO GTPases, RAS GTPase, and MAP kinases (ELMO2); Fcγ receptor (FCGR) dependent phagocytosis (ELMO2); VEGFA-VEGFR2 pathway (ELMO2)
	CD34	−.17	*ns*	*.615*	.77	**	*.007*		
	NF1	−.29	*ns*	*.381*	.71	*	*.018*		
	Phospho-AKT1 (S473)	−.12	*ns*	*.735*	.70	*	*.020*		
	CD68	−.04	*ns*	*.924*	.69	*	*.023*		
	BCL-XL	−.01	*ns*	*.99*	.68	*	*.025*		
	S6	.07	*ns*	*.839*	.66	*	*.031*		
	SMA	−.21	*ns*	*.539*	.66	*	*.031*		
	Fibronectin	−.04	*ns*	*.924*	.64	*	*.040*		
	EGFR	.03	*ns*	*.946*	.63	*	*.044*		
	VISTA	−.29	*ns*	*.386*	.62	*	*.048*		

AOI, area of interest; ns, not significant; WGCNA, weighted gene coexpression network analysis.

Statistical significance was determined using Spearman correlation test (*$P < .05$, **$P < .01$) in GraphPad Prism software v9.3.1. Graphed results are shown in Supplementary Figure 4.

[a]Genes with expression pattern best representative of combined module of coexpressed genes

[b]Enrichment pathway defined by Reactome and (genes in enriched pathway)